

New Physics in Rare B Decays after Moriond 2021

Wolfgang Altmannshofer^a, Peter Stangl^b

^a *Department of Physics and Santa Cruz Institute for Particle Physics,
University of California, Santa Cruz, 1156 High Street, Santa Cruz, CA 95064, United States*

^b *Albert Einstein Center for Fundamental Physics, Institute for Theoretical Physics,
University of Bern, Sidlerstrasse 5, CH-3012 Bern, Switzerland*

E-Mail: waltmann@ucsc.edu, stangl@itp.unibe.ch

The anomalies in rare B decays endure. We present results of an updated global analysis that takes into account the latest experimental input – in particular the recent results on R_K and $\text{BR}(B_s \rightarrow \mu^+ \mu^-)$ – and that qualitatively improves the treatment of theory uncertainties. Fit results are presented for the Wilson coefficients of four-fermion contact interactions. We find that muon specific Wilson coefficients $C_9 \simeq -0.82$ or $C_9 = -C_{10} \simeq -0.43$ continue to give an excellent description of the data. If only theoretically clean observables are considered, muon specific $C_{10} \simeq 0.60$ or $C_9 = -C_{10} \simeq -0.35$ both improve over the Standard Model by $\sqrt{\Delta\chi^2} \simeq 4.7\sigma$. In various new physics scenarios we provide predictions for lepton flavor universality observables and CP asymmetries that can be tested with more data. We update our previous combination of ATLAS, CMS, and LHCb data on $\text{BR}(B_s \rightarrow \mu^+ \mu^-)$ and $\text{BR}(B^0 \rightarrow \mu^+ \mu^-)$ taking into account the full two-dimensional non-Gaussian experimental likelihoods.

1. Introduction

Since several years there exist persistent discrepancies between the Standard Model (SM) predictions and the experimental results for rare decays of B mesons based on the neutral current $b \rightarrow s\ell\ell$ transitions. Discrepancies are seen in the branching fractions of the rare decays $B \rightarrow K\mu^+\mu^-$, $B \rightarrow K^*\mu^+\mu^-$, $B_s \rightarrow \phi\mu^+\mu^-$, and $B_s \rightarrow \mu^+\mu^-$, in the

angular distribution of $B \rightarrow K^* \mu^+ \mu^-$ and in lepton flavor universality (LFU) ratios. Of particular interest are the hints for LFU violation that have been observed by LHCb in the following ratios of branching fractions

$$R_K = \frac{\text{BR}(B \rightarrow K \mu^+ \mu^-)}{\text{BR}(B \rightarrow K e^+ e^-)}, \quad R_{K^*} = \frac{\text{BR}(B \rightarrow K^* \mu^+ \mu^-)}{\text{BR}(B \rightarrow K^* e^+ e^-)}. \quad (1)$$

While the SM predictions for most absolute branching fractions and also the angular observables are potentially subject to large hadronic uncertainties, the LFU ratios R_K and R_{K^*} can be predicted with high accuracy. Significant deviations in these observables would thus constitute clean indirect evidence for new physics. Also the absolute branching ratio of the purely leptonic decay $B_s \rightarrow \mu^+ \mu^-$ can be considered as theoretically clean. Non-perturbative physics enters through a single hadronic parameter, the B_s meson decay constant, which is known with high precision from lattice QCD calculations.

Intriguingly, the simplest new physics scenarios that address the theoretically clean hints for LFU violation simultaneously explain also the other discrepancies. Parameterizing the new physics in terms of four fermion contact interactions, global fits of rare B decay data find consistently very strong preference for new physics in the form of the operator $\frac{1}{\Lambda_{\text{NP}}^2}(\bar{s}\gamma_\alpha P_L b)(\bar{\mu}\gamma^\alpha \mu)$ or $\frac{1}{\Lambda_{\text{NP}}^2}(\bar{s}\gamma_\alpha P_L b)(\bar{\mu}\gamma^\alpha P_L \mu)$ with a generic new physics scale of $\Lambda_{\text{NP}} \simeq 35$ TeV (for recent work see [1–10]).

Very recently, the LHCb collaboration presented updated results for two theoretically clean observables that have previously shown tensions with the SM predictions: the LFU ratio R_K and the branching ratio $\text{BR}(B_s \rightarrow \mu^+ \mu^-)$. Using the full run 2 data set the value for R_K is [11]

$$R_K = 0.846^{+0.042}_{-0.039} {}^{+0.013}_{-0.012}, \quad \text{for } 1.1 \text{ GeV}^2 < q^2 < 6 \text{ GeV}^2, \quad (2)$$

where the first uncertainty is statistical and the second one systematic, and q^2 is the dimuon invariant mass squared. The new result has exactly the same central value as the previous result $R_K = 0.846^{+0.060+0.016}_{-0.054-0.014}$ [12], while the uncertainty has been reduced by a factor of roughly 2/3. Consequently, the tension between the experimental measurement and the SM prediction, which is unity to an excellent approximation, has increased from previously 2.5σ to now 3.1σ .

The branching ratio of the $B_s \rightarrow \mu^+ \mu^-$ decay measured with the full run 2 data is found to be [13]

$$\overline{\text{BR}}(B_s \rightarrow \mu^+ \mu^-) = (3.09^{+0.46}_{-0.43} {}^{+0.15}_{-0.11}) \times 10^{-9}, \quad (3)$$

where the first uncertainty is statistical and the second one systematic. This result by itself has a precision close to the previous world average $\text{BR}(B_s \rightarrow \mu^+ \mu^-) = (2.69^{+0.37}_{-0.35}) \times$

10^{-9} [14] that was based on results from ATLAS, CMS, and LHCb [15–17]. Compared to the previous measurement by LHCb, $\text{BR}(B_s \rightarrow \mu^+ \mu^-) = (3.0 \pm 0.6_{-0.2}^{+0.3}) \times 10^{-9}$ [15], the new update finds nearly the same central value. While the LHCb result is compatible with the SM prediction within 1σ , the previous world average was below the SM prediction by more than 2σ . Here, we provide an update of the world average of the $B_s \rightarrow \mu^+ \mu^-$ branching ratio and the correlated $B^0 \rightarrow \mu^+ \mu^-$ branching ratio, taking into account the new LHCb results. A Gaussian approximation to our combined two-dimensional likelihood is given by

$$\overline{\text{BR}}(B_s \rightarrow \mu^+ \mu^-)_{\text{exp}} = (2.93 \pm 0.35) \times 10^{-9}, \quad (4)$$

$$\text{BR}(B^0 \rightarrow \mu^+ \mu^-)_{\text{exp}} = (0.56 \pm 0.70) \times 10^{-10}, \quad (5)$$

with an error correlation coefficient $\rho = -0.27$. We find a tension with the SM predictions of 2.3σ . Details on how the combination and the discrepancy with the SM are obtained are given in the appendix A.

The main goal of this paper is to interpret the impact of the new experimental results in a model independent way, using the well established effective Hamiltonian approach. We parameterize new physics contributions by Wilson coefficients of dimension 6 interactions evaluated at the renormalization scale $\mu = 4.8 \text{ GeV}$

$$\mathcal{H}_{\text{eff}} = \mathcal{H}_{\text{eff}}^{\text{SM}} - \frac{4G_F}{\sqrt{2}} V_{tb} V_{ts}^* \frac{e^2}{16\pi^2} \sum_{\ell=e,\mu} \sum_{i=9,10,S,P} (C_i^{bs\ell\ell} O_i^{bs\ell\ell} + C_i'^{bs\ell\ell} O_i'^{bs\ell\ell}) + \text{h.c.} \quad (6)$$

We consider the following set of semi-leptonic operators

$$O_9^{bs\ell\ell} = (\bar{s}\gamma_\mu P_L b)(\bar{\ell}\gamma^\mu \ell), \quad O_9'^{bs\ell\ell} = (\bar{s}\gamma_\mu P_R b)(\bar{\ell}\gamma^\mu \ell), \quad (7)$$

$$O_{10}^{bs\ell\ell} = (\bar{s}\gamma_\mu P_L b)(\bar{\ell}\gamma^\mu \gamma_5 \ell), \quad O_{10}'^{bs\ell\ell} = (\bar{s}\gamma_\mu P_R b)(\bar{\ell}\gamma^\mu \gamma_5 \ell), \quad (8)$$

$$O_S^{bs\ell\ell} = m_b(\bar{s}P_R b)(\bar{\ell}\ell), \quad O_S'^{bs\ell\ell} = m_b(\bar{s}P_L b)(\bar{\ell}\ell), \quad (9)$$

$$O_P^{bs\ell\ell} = m_b(\bar{s}P_R b)(\bar{\ell}\gamma_5 \ell), \quad O_P'^{bs\ell\ell} = m_b(\bar{s}P_L b)(\bar{\ell}\gamma_5 \ell). \quad (10)$$

We do not consider semi-leptonic tensor operators, because they are not generated at dimension 6 in the Standard Model Effective Field Theory (SMEFT). Similarly, in the case of the scalar operators, we will impose the following relations among the corresponding Wilson coefficients $C_S^{bs\ell\ell} = -C_P^{bs\ell\ell}$ and $C_S'^{bs\ell\ell} = C_P'^{bs\ell\ell}$, as they hold at dimension 6 in the SMEFT [18]. We also do not consider semi-tauonic operators or 4-quark operators, as they affect the observables we consider only at the loop level [19, 20].

A critical aspect of global fits is the treatment of theory uncertainties. In our previous studies [6, 21–23] we have evaluated theory uncertainties and their correlations for the

Wilson coefficients fixed to their SM values. This is typically a good approximation as long as the best fit results are in the vicinity of the SM point. Possible exceptions are observables that have negligible uncertainties in the SM but not in the presence of new physics contributions. A prominent example of such observables are the LFU ratios R_K and R_{K^*} . While the experimental uncertainties still dominate for R_K and R_{K^*} , the precision of the new R_K result in eq. (2) is strong motivation to improve our treatment of theory uncertainties. In this paper we incorporate the new physics dependence of the theory uncertainties for the first time in our fit.

The paper is organized as follows: in section 2 we discuss in detail the improved treatment of theory uncertainties and illustrate the size of the effect in the case of LFU observables and CP asymmetries in the presence of new physics. In section 3 we collect the results of the updated global fit. We consider scenarios with one real Wilson coefficient at a time, scenarios with two real Wilson coefficients as well as scenarios with complex Wilson coefficients. Section 4 contains new physics predictions for a number of LFU observables and CP asymmetries that can be tested with future data. We conclude in section 5. Our combination of the experimental results on the $B_s \rightarrow \mu^+ \mu^-$ branching ratio is described in appendix A.

2. Improved Treatment of Theory Uncertainties

Our global fits are based on a χ^2 function that depends on the Wilson coefficients in the effective Hamiltonian and that takes into account both the theoretical and experimental uncertainties in terms of covariance matrices, C_{exp} and C_{th}

$$\chi^2(C_i) = \left(\vec{O}_{\text{exp}} - \vec{O}_{\text{th}}(C_i) \right)^T \left(C_{\text{exp}} + C_{\text{th}} \right)^{-1} \left(\vec{O}_{\text{exp}} - \vec{O}_{\text{th}}(C_i) \right). \quad (11)$$

In the above expression, the \vec{O}_{exp} are the measured central values of the observables of interest and \vec{O}_{th} are the corresponding theory predictions that have dependence on the considered set of Wilson coefficients C_i . In previous global fits, we made the assumption that the theoretical uncertainties are well described by the covariance matrix C_{th} determined with the SM values for the Wilson coefficients and neglected possible dependence of C_{th} on the new physics. This has the advantage that the time consuming evaluation of C_{th} has to be performed only once.

We developed a computationally efficient method to determine the new physics dependence of C_{th} . As the rare B decay amplitudes are linear functions of the Wilson coefficients it is possible to express the branching ratios as second order polynomials in the Wilson coefficients. The coefficients of the polynomials are independent of new

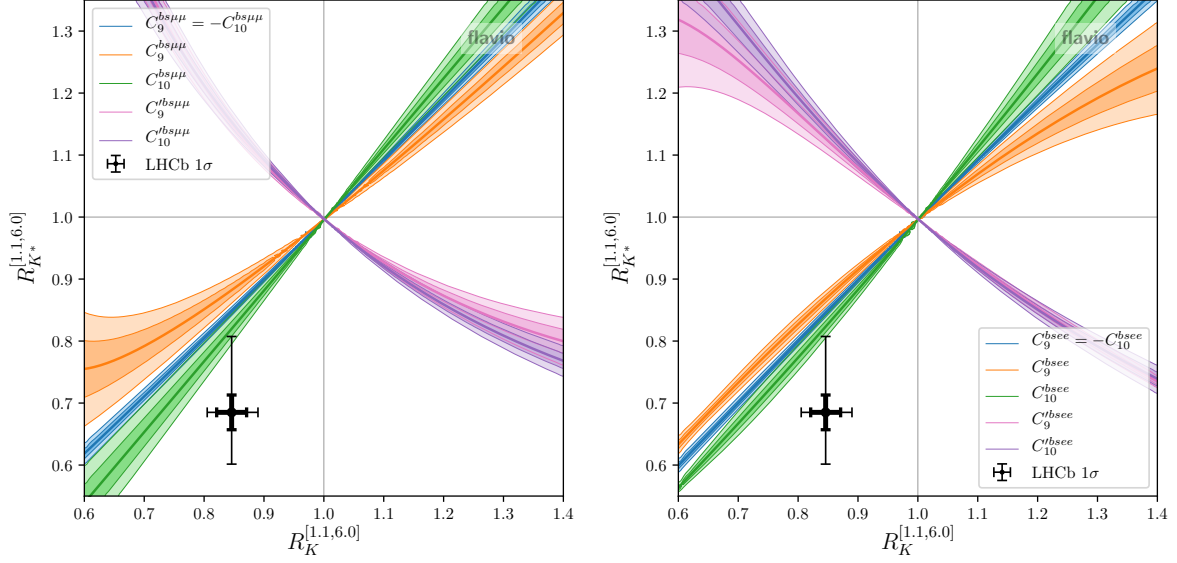


Figure 1: Theory predictions for R_K and R_{K^*} in the presence of various non-standard Wilson coefficients (left: new physics in muons; right: new physics in electrons). The colored bands correspond to the 1σ and 2σ theory uncertainties. Also shown are the current experimental results (thin error bars) and the expected experimental precision after run 3 of the LHC (bold error bars).

physics and their correlated uncertainties can be described by a covariance matrix that needs to be determined only once. The covariance matrix of the branching ratios can then be expressed in a straight forward way in terms of the covariance matrix of the polynomial coefficients and the Wilson coefficients.

The CP averaged angular observables S_i , the CP asymmetries A_i , and the LFU ratios can be written in terms of ratios of second order polynomials, while the P'_i observables involve also irrational functions. In those cases we obtain an approximation of the covariance matrix for the observables by expanding the functions to second order in the Wilson coefficients and then following the same procedure as for the branching ratios. We find that this procedure gives reliable estimates as long as the absolute values of the new physics Wilson coefficients are somewhat smaller than the corresponding relevant SM coefficients. In principle, the accuracy of the approximation could be systematically improved by expanding to higher orders.

The new error treatment is particularly relevant for quantities that are predicted with very high precision in the SM but that have non-negligible uncertainties in the presence of new physics. In that case, the corresponding entries in the theoretical covariance

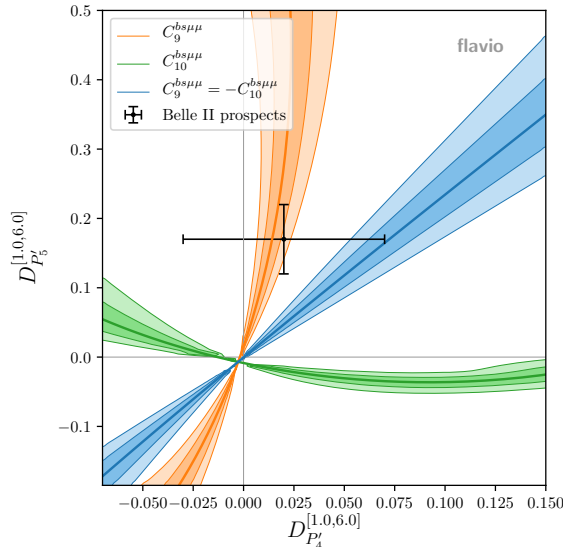


Figure 2: Theory predictions for $D_{P'_4}$ and $D_{P'_5}$ in the presence of few non-standard Wilson coefficients. The colored bands correspond to the 1σ and 2σ theory uncertainties. Also shown is the expected experimental precision with the full Belle II data set assuming a new physics benchmark point (bold error bars).

matrix evaluated in the SM and the ones in the presence of new physics may differ significantly. The most important examples can be grouped into three categories: (i) lepton flavor universality tests, (ii) CP asymmetries, (iii) observables that vanish in the absence of right-handed currents. In most cases, the current experimental uncertainties of these observables are considerably larger than the theory uncertainties both in the SM as well as in viable new physics scenarios and the impact of the theory uncertainties in the global is moderate. However, with the expected improvement in experimental sensitivity, the theoretical uncertainties will become more and more important and their new physics dependence needs to be taken into account.

Among the lepton universality tests, ratios of branching ratios, like R_K and R_{K^*} , are known with high precision in the SM, with uncertainties of around 1% [24, 25]. In the presence of new physics, however, the uncertainties can be several percent. On the experimental side, the most precisely known quantity is R_K , with an uncertainty of $\sim 4\%$ [11], c.f. eq. (2). After run 3 of the LHC, with $\sim 25 \text{ fb}^{-1}$ of integrated luminosity collected by LHCb, one expects an experimental uncertainty of R_K (R_{K^*}) of $\sim 2.5\%$ (2.8%) [26] assuming that systematic uncertainties can be controlled. The precision might reach $\sim 1\%$ with 300 fb^{-1} . This clearly shows the need to consistently take into account the theory uncertainties including their new physics dependence. Other lepton

universality tests, like the differences of angular observables $D_{P'_i} = P'_i(B \rightarrow K^* \mu \mu) - P'_i(B \rightarrow K^* e e)$ [27] (denoted by Q_i in [28, 29]), have currently sizeable experimental uncertainties [29] and do not play a major role in global fits, yet. However, given the expected future experimental precision of a few percent [26] it becomes desirable to have a robust treatment of their theory uncertainties as well.

In Figures 1 and 2 we illustrate the above points with a few examples. The plots in Figure 1 show the theory predictions for R_K and R_{K^*} (in the q^2 bin from 1.1 GeV² to 6 GeV²) in the presence of new physics parameterized by various Wilson coefficients. As is well known, the Wilson coefficients with left-handed quark currents (C_9 and C_{10}) lead to a correlated effect in R_K and R_{K^*} , while for right-handed quark currents (C'_9 and C'_{10}) one finds an anti-correlation [30]. For $C_9 = -C_{10}$ one has to an excellent approximation $R_K \simeq R_{K^*}$. The various colored bands show the theoretical uncertainties at the 1σ and 2σ level. While the uncertainties are negligible close to the SM point, they become sizeable away from it. For comparison, we also show the current experimental results with 1σ uncertainties [11, 31], as well as the expected uncertainties after run 3, assuming the same central value.

Similarly, the plot in Figure 2 shows the theory predictions for $D_{P'_4}$ and $D_{P'_5}$ (in the q^2 bin from 1 GeV² to 6 GeV²) in the presence of a few combinations of non standard Wilson coefficients. Also here we observe that the theory uncertainties can be sizable away from the SM point. As the current experimental uncertainties are still large [29], we show as comparison the expected experimental uncertainties with the full Belle II data-set which we expect to be around 5%¹, assuming as central value the prediction of a new physics benchmark point $(C_9^{bs\mu\mu}, C_{10}^{bs\mu\mu}) \simeq (-0.67, 0.24)$.

With regards to CP violation, we note that results on CP asymmetries in $B \rightarrow K^* \mu^+ \mu^-$ are available from LHCb with 3fb⁻¹ of run 1 data [32]. The most interesting asymmetries are A_7 , A_8 , and A_9 as they are not suppressed by small strong phases and therefore could in principle be $\mathcal{O}(1)$ in the presence of CP violating new physics [33]. In the SM, they are strongly Cabibbo suppressed, $A_7, A_8 \sim \mathcal{O}(10^{-3})$ [34]. The available experimental results are all compatible with zero with uncertainties of approximately 5% [32] both at low $q^2 \in (1 \text{ GeV}^2, 6 \text{ GeV}^2)$ and at high $q^2 \in (15 \text{ GeV}^2, 19 \text{ GeV}^2)$. Scaling with \sqrt{N} , we expect sensitivities with the run 2 data set of approximately 2% – 3% and ultimate sensitivities of below 1% with 300fb⁻¹.

In Figure 3 we show the theory predictions for the $B \rightarrow K^* \mu^+ \mu^-$ CP asymmetries A_7 and A_8 (in the q^2 bin from 1.1 GeV² to 6 GeV²) in the presence of imaginary parts

¹This value is informed by the expected sensitivities for $P'_{4,5}$ given in [26] and assumes that $D_{P'_{4,5}}$ can be measured with similar precision.

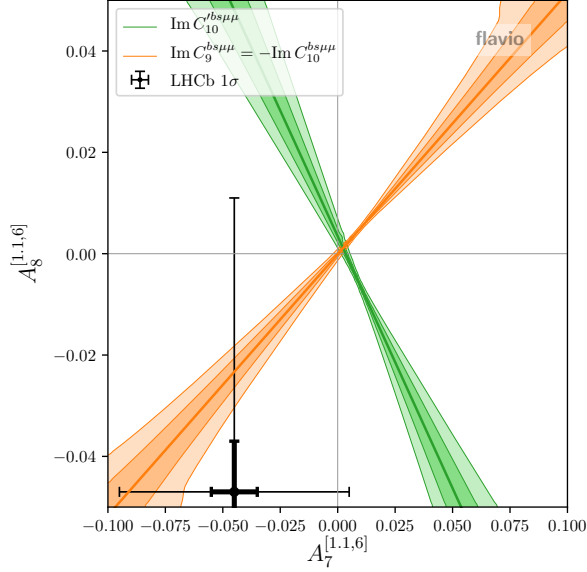


Figure 3: Theory predictions for A_7 and A_8 in the presence of imaginary Wilson coefficients. The colored bands correspond to the 1σ and 2σ theory uncertainties. Also shown are the current experimental results (thin error bars) and a experimental precision goal of 1% (bold error bars).

of Wilson coefficients. Similarly to the LFU observables discussed above, also here we observe non-negligible theory uncertainties away from the SM point. For comparison, we also show the current experimental results with 1σ uncertainties [32], as well as uncertainties of 1%, assuming the same central value.

3. The Updated Global Fit

In comparison to our previous fit in [6], we improve the treatment of the theory uncertainties as described in the previous section and we include a series of new experimental results:

- The update of the $B^0 \rightarrow K^{*0} \mu^+ \mu^-$ angular analysis with 2016 data from LHCb [35]. The P'_5 anomaly persists in this recent update, with a slightly reduced significance compared to the run 1 results [32].
- The new $B^\pm \rightarrow K^{*\pm} \mu^+ \mu^-$ angular analysis [36]. While the experimental uncertainties of the $B^\pm \rightarrow K^{*\pm} \mu^+ \mu^-$ angular analysis are still sizeable, deviations from SM predictions are observed that are broadly showing the same pattern as in the $B^0 \rightarrow K^{*0} \mu^+ \mu^-$ angular analysis.

- The latest results on $B_s \rightarrow \mu^+ \mu^-$ from CMS [17] and the very recent result from LHCb [13]. We combine these results with the ATLAS result [16], as described in appendix A. Compared to the previous LHC combination [14], our combination has a slightly large central value and a slightly reduced relative uncertainty.
- The recent update of R_K [11]. The new result has exactly the same central value but reduced uncertainty compared to the previous result [12], increasing the tension with the SM from 2.5σ to 3.1σ .

In our global fit we do not include the recent result from LHCb [13] on the effective $B_s \rightarrow \mu^+ \mu^-$ lifetime, $\tau_{\text{eff}} = (2.07 \pm 0.29 \pm 0.03) \times 10^{-12}$ s (see [15, 17] for previous results on the effective lifetime). This result can be translated into the mass eigenstate rate asymmetry [37, 38]

$$A_{\Delta\Gamma} = \frac{1}{y_s} \frac{(1 - y_s^2)\tau_{\text{eff}} - (1 + y_s^2)\tau_{B_s}}{2\tau_{B_s} - (1 - y_s^2)\tau_{\text{eff}}}, \quad (12)$$

where $\tau_{B_s} = (1.513 \pm 0.009) \times 10^{-12}$ [39] is the B_s mean lifetime and $y_s = \tau_{B_s} \Delta\Gamma_s/2 = (6.5 \pm 0.3)\%$ [39] is related to the B_s width difference. Using the LHCb result for τ_{eff} , we find $A_{\Delta\Gamma} = 8.6 \pm 7.2$, which includes at 2σ the entire physical range $-1 \leq A_{\Delta\Gamma} \leq 1$. Future precision measurements of τ_{eff} could lead to non-trivial constraints on new physics in the form of the scalar Wilson coefficients $C_{S,P}^{(\prime)}$ [37, 38].

Our numerical code is based on the Python package `flavio` [40], which provides all the theory predictions including their uncertainties and correlations. We use the full set of $b \rightarrow s\ell\ell$ observables and measurements as implemented in the Python package `smelli` [41, 42], which builds upon `flavio`. We plan to implement our new error treatment (cf. section 2) in future versions of `flavio` and `smelli`.

3.1. One parameter scenarios

We start by considering simple one parameter new physics scenarios, switching on one real new physics Wilson coefficient at a time. We consider several fits, including certain subsets of observables. In Table 1 we report the best fit values for the Wilson coefficients as well as the 1σ best-fit regions and the “pull” in σ , defined as the $\sqrt{\Delta\chi^2}$ between the best fit point and the χ^2 of the SM.

In the column “ $b \rightarrow s\mu\mu$ ” in Table 1, we focus on the $b \rightarrow s\mu\mu$ observables that include the differential branching ratios of $B \rightarrow K\mu^+\mu^-$, $B \rightarrow K^*\mu^+\mu^-$, $B_s \rightarrow \phi\mu^+\mu^-$, and $\Lambda_b \rightarrow \Lambda\mu^+\mu^-$ as well as all available CP averaged angular observables in these decays. Note that these observables are subject to potentially large hadronic uncertainties. While existing calculations indicate that long distance effects are well within the assumed

Wilson coefficient	$b \rightarrow s\mu\mu$		LFU, $B_s \rightarrow \mu\mu$		all rare B decays	
	best fit	pull	best fit	pull	best fit	pull
$C_9^{bs\mu\mu}$	$-0.91^{+0.18}_{-0.17}$	4.9σ	$-0.74^{+0.20}_{-0.21}$	4.1σ	$-0.82^{+0.14}_{-0.14}$	6.2σ
$C_{10}^{bs\mu\mu}$	$+0.51^{+0.23}_{-0.24}$	2.0σ	$+0.60^{+0.14}_{-0.13}$	4.7σ	$+0.56^{+0.12}_{-0.12}$	4.9σ
$C_9^{bbs\mu\mu}$	$+0.55^{+0.26}_{-0.25}$	2.2σ	$-0.31^{+0.16}_{-0.17}$	2.0σ	$-0.09^{+0.13}_{-0.13}$	0.7σ
$C_{10}^{bbs\mu\mu}$	$-0.15^{+0.16}_{-0.16}$	0.9σ	$+0.05^{+0.12}_{-0.12}$	0.4σ	$+0.01^{+0.10}_{-0.09}$	0.1σ
$C_9^{bs\mu\mu} = C_{10}^{bs\mu\mu}$	$-0.41^{+0.15}_{-0.15}$	2.7σ	$+0.43^{+0.18}_{-0.18}$	2.5σ	$-0.06^{+0.11}_{-0.11}$	0.5σ
$C_9^{bs\mu\mu} = -C_{10}^{bs\mu\mu}$	$-0.65^{+0.12}_{-0.12}$	4.9σ	$-0.35^{+0.08}_{-0.08}$	4.7σ	$-0.43^{+0.07}_{-0.07}$	6.2σ
C_9^{bsee}			$+0.74^{+0.20}_{-0.19}$	4.1σ	$+0.75^{+0.20}_{-0.19}$	4.1σ
C_{10}^{bsee}			$-0.67^{+0.17}_{-0.18}$	4.2σ	$-0.66^{+0.16}_{-0.17}$	4.3σ
C_9^{bse}			$+0.35^{+0.18}_{-0.17}$	2.1σ	$+0.39^{+0.19}_{-0.18}$	2.3σ
C_{10}^{bse}			$-0.31^{+0.16}_{-0.16}$	2.0σ	$-0.29^{+0.15}_{-0.16}$	2.0σ
$C_9^{bsee} = C_{10}^{bsee}$			$-1.40^{+0.26}_{-0.26}$	4.0σ	$-1.28^{+0.24}_{-0.23}$	4.1σ
$C_9^{bsee} = -C_{10}^{bsee}$			$+0.37^{+0.10}_{-0.10}$	4.2σ	$+0.37^{+0.10}_{-0.10}$	4.3σ
$(C_S^{bs\mu\mu} = -C_P^{bs\mu\mu}) \times \text{GeV}$			$-0.004^{+0.002}_{-0.002}$	2.2σ	$-0.003^{+0.002}_{-0.002}$	1.5σ
$(C_S^{bbs\mu\mu} = C_P^{bbs\mu\mu}) \times \text{GeV}$			$-0.004^{+0.002}_{-0.002}$	2.2σ	$-0.003^{+0.002}_{-0.002}$	1.5σ

Table 1: Best-fit values with corresponding 1σ ranges as well as pulls in sigma between the best-fit point and the SM point for scenarios with NP in a single real Wilson coefficient. Column “ $b \rightarrow s\mu\mu$ ”: fit including only the $b \rightarrow s\mu\mu$ observables (branching ratios and angular observables). Column “LFU, $B_s \rightarrow \mu\mu$ ”: fit including only the neutral current LFU observables ($R_{K^{(*)}}$, $D_{P'_{4,5}}$) and $\text{BR}(B_s \rightarrow \mu^+\mu^-)$. In column “all rare B decays”, we show the results of the combined fit. For the scalar Wilson coefficients, the SM-like solution is shown, while a sign-flipped solution is also allowed [38].

uncertainties [43], it cannot be fully excluded that such effects are unexpectedly large. As the considered decay modes do neither involve electrons nor are sensitive to scalar operators, only results for vector and axial-vector muonic Wilson coefficients are shown. Consistent with previous findings, we observe that a negative $C_9^{bs\mu\mu} \simeq -0.91$ or the left-handed muon combination $C_9^{bs\mu\mu} = -C_{10}^{bs\mu\mu} \simeq -0.65$, are strongly preferred by the fit. For those values of the Wilson coefficients the agreement between theory and data is improved by nearly 5σ compared to the SM

In the column “LFU, $B_s \rightarrow \mu\mu$ ” in Table 1, we consider the neutral current LFU observables ($R_{K^{(*)}}$, $D_{P'_{4,5}}$) and $\text{BR}(B_s \rightarrow \mu^+\mu^-)$ only, including in particular the new R_K and $\text{BR}(B_s \rightarrow \mu^+\mu^-)$ result. The included observables are considered under excellent theoretical control and the discrepancies cannot be explained by hadronic effects. Two scenarios stand out, $C_{10}^{bs\mu\mu} \simeq +0.6$ and $C_9^{bs\mu\mu} = -C_{10}^{bs\mu\mu} \simeq -0.35$, which both have a pull of 4.7σ . These scenarios do not only address the anomalies in R_K and R_{K^*} , but also the slightly reduced branching ratio of $B_s \rightarrow \mu^+\mu^-$. The coefficients $C_9^{bs\mu\mu}$, C_9^{bsee} , and C_{10}^{bsee} can explain the R_K and R_{K^*} data, but do not affect the $B_s \rightarrow \mu^+\mu^-$ decay. Their pulls are therefore a bit lower, around 4σ . The scalar Wilson coefficients show a slight ($\sim 2\sigma$) preference for negative values, that lead to a suppression of the $B_s \rightarrow \mu\mu$ branching ratio in accordance with the data.

Finally, in the the column “all rare B decays” in Table 1 we show the results of the global fit. Included are the $b \rightarrow s\mu\mu$ observables, the LFU observables, and the $B_s \rightarrow \mu^+\mu^-$ branching ratio.² The largest pulls of 6.2σ are found for $C_9^{bs\mu\mu} \simeq -0.82$ and $C_9^{bs\mu\mu} = -C_{10}^{bs\mu\mu} \simeq -0.43$. As expected, the pulls for the electronic Wilson coefficients and the scalar Wilson coefficients are very similar to the values in the “LFU, $B_s \rightarrow \mu\mu$ ” column.

3.2. Two parameter scenarios

Next, we discuss scenarios where two Wilson coefficients are turned on simultaneously. In Figure 4 we show the best fit regions in the $C_9^{bs\mu\mu}$ vs. $C_{10}^{bs\mu\mu}$ plane. The plot on the left focuses on the constraints from the LFU ratios R_K and R_{K^*} . The R_K constraint before the update [11] is shown by the dashed contours. As the measured $R_K > R_{K^*}$ the best fit range prefers a sizable positive $C_{10}^{bs\mu\mu}$. The plot on the right shows the result of the global fit. The $B_s \rightarrow \mu^+\mu^-$ branching ratio prefers a modest positive $C_{10}^{bs\mu\mu}$, while the $b \rightarrow s\mu\mu$ observables mainly prefer a negative $C_9^{bs\mu\mu}$. Overall, the best fit point

²Note that in previous fits [6] we had also included $\Delta F = 2$ observables that are correlated to the $B_s \rightarrow \mu^+\mu^-$ branching ratio and the various $b \rightarrow s\mu\mu$ branching ratio, mainly through their dependence on common CKM input. Adding $\Delta F = 2$ observables in the fit further increases the pulls slightly.

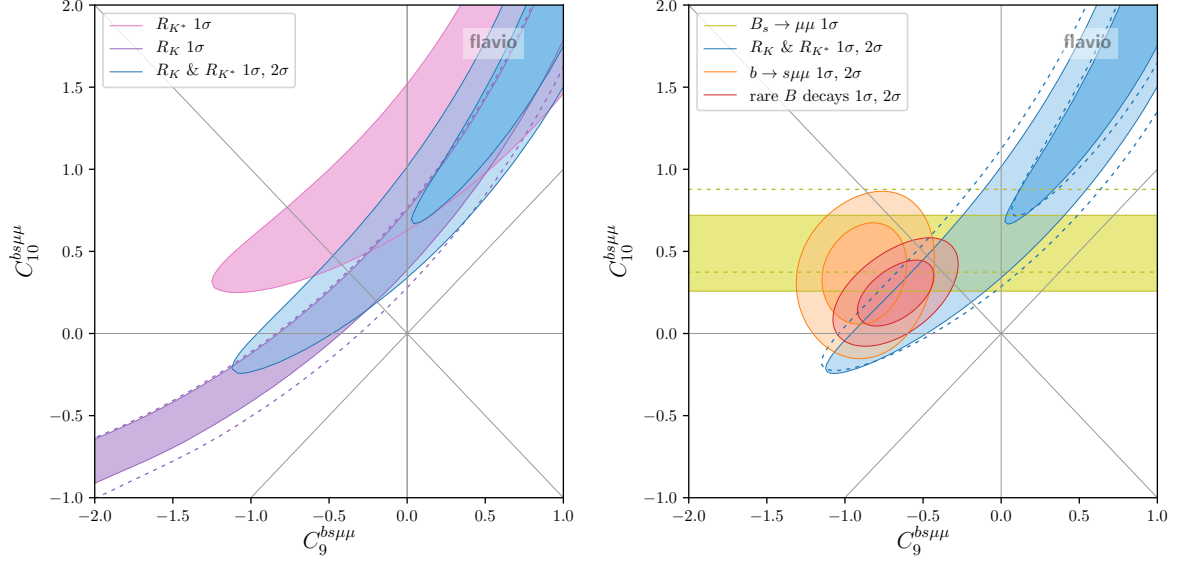


Figure 4: Constraints in the Wilson coefficient plane $C_9^{bs\mu\mu}$ vs. $C_{10}^{bs\mu\mu}$. Left: LFU ratios only. Right: Combination of LFU ratios, combination of $b \rightarrow s\mu\mu$ observables, $\text{BR}(B_s \rightarrow \mu^+\mu^-)$, and the global fit. The dashed lines show the constraints before the recent updates [11, 13].

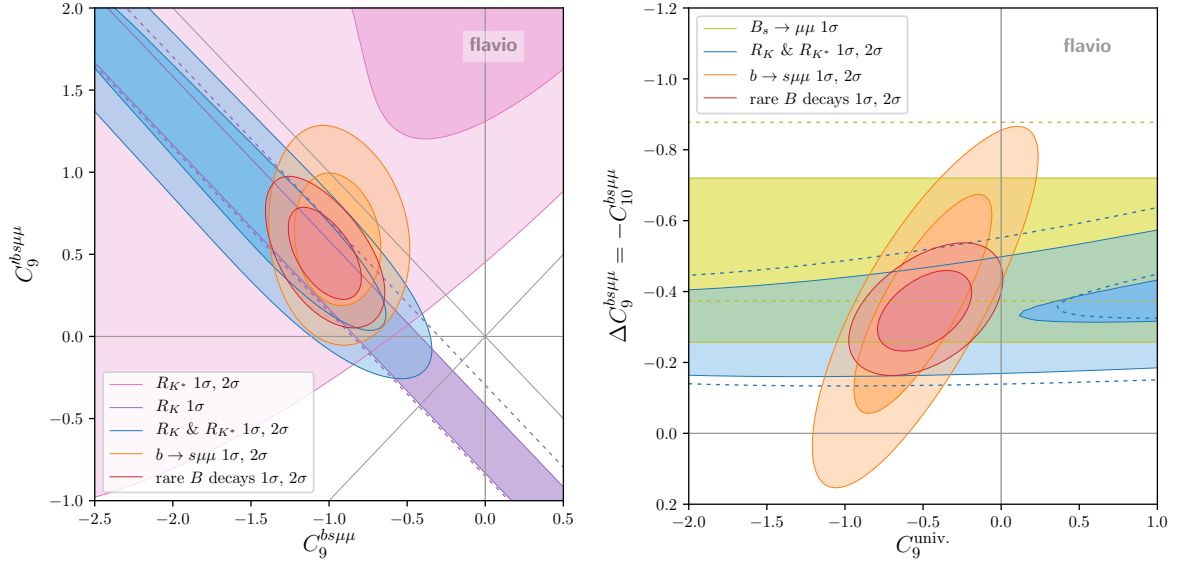


Figure 5: Constraints in the Wilson coefficient planes $C_9^{bs\mu\mu}$ vs. $C_9^{bs\mu\mu}$ (left) and $C_9^{bs\mu\mu}$ vs. $\Delta C_9^{bs\mu\mu} = -C_{10}^{bs\mu\mu}$ (right). The dashed lines show the constraints before the recent updates [11, 13].

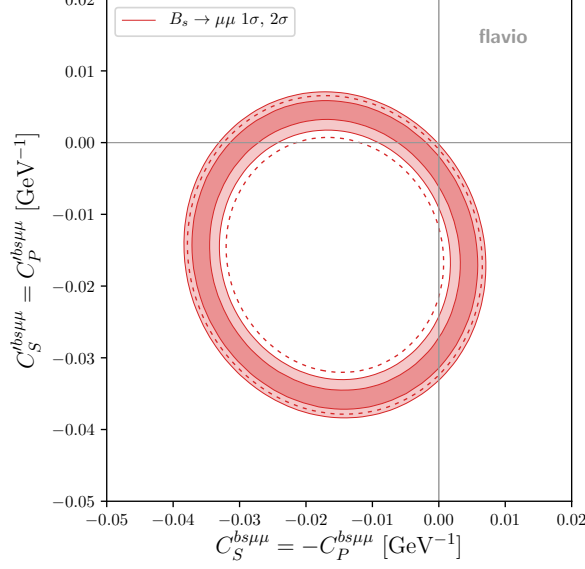


Figure 6: Constraint in the Wilson coefficient plane $C_S^{bs\mu\mu} = -C_P^{bs\mu\mu}$ vs. $C_S^{bs\mu\mu} = C_P^{bs\mu\mu}$. The red band shows at 1σ and 2σ the constraints for $(C_{10}^{bs\mu\mu}, C_{10}^{bs\mu\mu}) = (0, 0)$. The dashed lines show the constraints before the recent update [13].

corresponds to $(C_9^{bs\mu\mu}, C_{10}^{bs\mu\mu}) \simeq (-0.67, 0.24)$ with a pull of 6.1σ .

In Figure 5 we show the viable parameter space of a couple of other Wilson coefficient pairs, that were found to give good fits in the past. The plot on the left shows the $C_9^{bs\mu\mu}$ vs. $C_9^{bs\mu\mu}$ plane, while the plot on the right shows the $C_9^{\text{univ.}}$ vs. $\Delta C_9^{bs\mu\mu} = -C_{10}^{bs\mu\mu}$ plane (defined such that $C_9^{bsee} = C_9^{\text{univ.}}$ and $C_9^{bs\mu\mu} = C_9^{\text{univ.}} + \Delta C_9^{bs\mu\mu}$). The best fit points are given by $(C_9^{bs\mu\mu}, C_9^{bs\mu\mu}) \simeq (-1.03, 0.50)$ and $(C_9^{\text{univ.}}, \Delta C_9^{bs\mu\mu}) \simeq (-0.50, -0.34)$ and correspond to pulls of 6.5σ and 6.4σ , respectively. The scenario on the left gives an excellent fit of R_K and R_{K^*} , but the slightly reduced $B_s \rightarrow \mu^+ \mu^-$ branching ratio remains unexplained. The scenario on the right can resolve the tension in $\text{BR}(B_s \rightarrow \mu^+ \mu^-)$, but leaves a tension between R_K and R_{K^*} . Note that $C_9^{\text{univ.}}$ could in principle be mimicked by a hadronic effect.

As clearly seen in the plots of Figures 4 and 5, the branching ratio of $B_s \rightarrow \mu^+ \mu^-$ plays an important role in constraining the Wilson coefficient C_{10} . It is well known that $B_s \rightarrow \mu^+ \mu^-$ is also very sensitive to new physics in the scalar Wilson coefficients (see e.g. [38]). In Figure 6 we show the constraints in the Wilson coefficient plane $C_S^{bs\mu\mu} = -C_P^{bs\mu\mu}$ vs. $C_S^{bs\mu\mu} = C_P^{bs\mu\mu}$ based on our combination of the experimental results on $\text{BR}(B_s \rightarrow \mu^+ \mu^-)$. The red band shows the 1σ and 2σ constraint when the semileptonic new physics coefficients $C_{10}^{bs\mu\mu}$ and $C_{10}^{bs\mu\mu}$ are set to zero. The $\sim 2\sigma$ tension between the $\text{BR}(B_s \rightarrow \mu^+ \mu^-)$ SM prediction and the experimental world average is

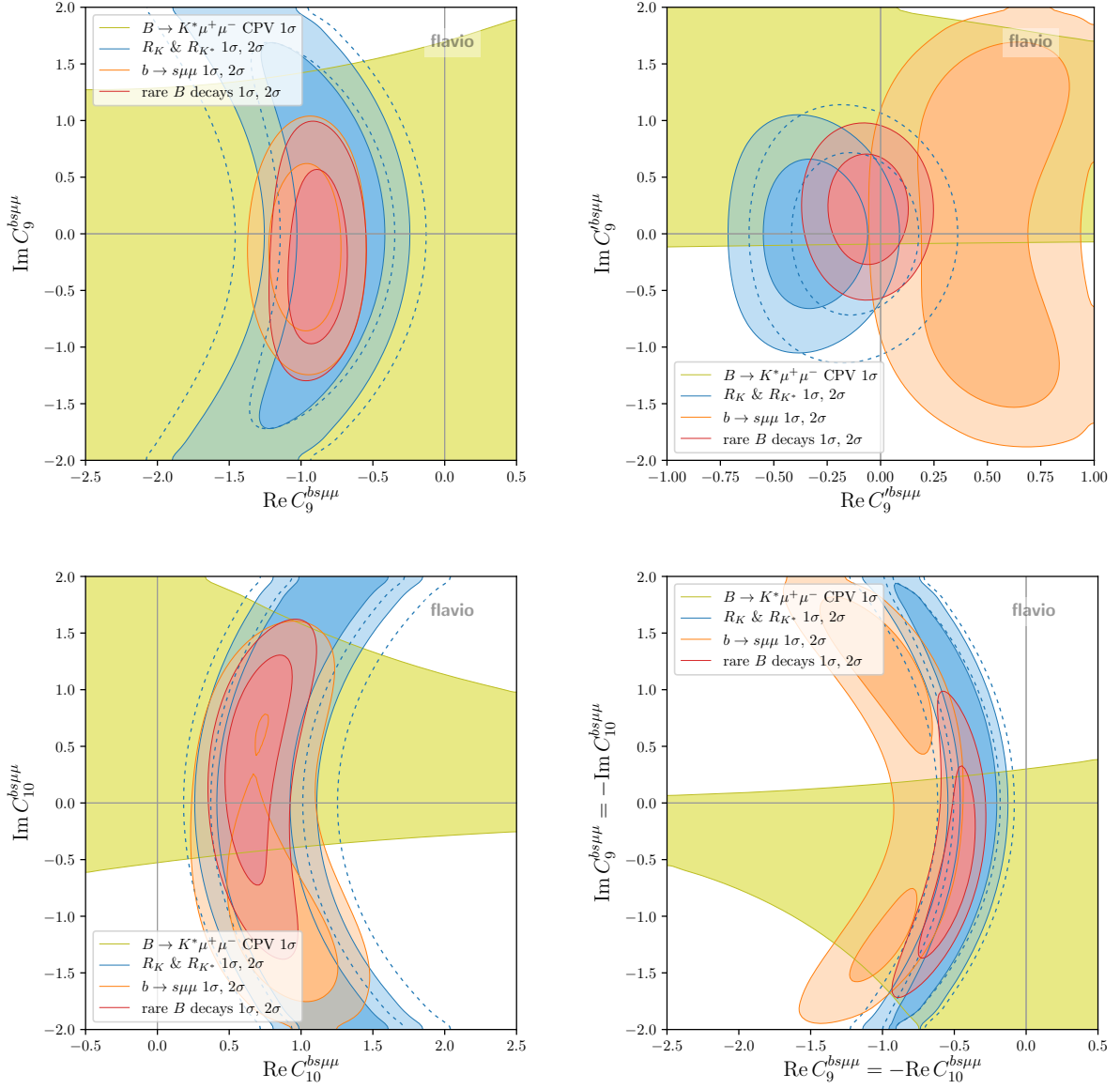


Figure 7: Constraints in the planes of complex $C_9^{bs\mu\mu}$ (top left), $C_9'^{bs\mu\mu}$ (top right), $C_{10}^{bs\mu\mu}$ (bottom left), and $C_9^{bs\mu\mu} = -C_{10}^{bs\mu\mu}$ (bottom right). Shown separately are the constraints from LFU observables, CP conserving $b \rightarrow s \mu \mu$ observables, the $B \rightarrow K^* \mu^+ \mu^-$ CP asymmetries, and the global fit. The dashed lines show the constraints before the recent update [11].

clearly reflected in the plot. With the recent $\text{BR}(B_s \rightarrow \mu^+\mu^-)$ update, the preferred region in the Wilson coefficient space moved slightly towards the SM point.

3.3. Complex Wilson Coefficients

In the presence of new physics, the contributions to the flavor changing Wilson coefficients can generically be CP violating. While the observables that show tensions with SM predictions are CP conserving, it is interesting to investigate the impact that imaginary parts of Wilson coefficients have on the fit, and to which extent imaginary parts are constrained by existing data.

In Figure 7 we show constraints in the planes of complex $C_9^{bs\mu\mu}$ (top left), $C_9'^{bs\mu\mu}$ (top right), $C_{10}^{bs\mu\mu}$ (bottom left), and $C_9^{bs\mu\mu} = -C_{10}^{bs\mu\mu}$ (bottom right). Shown separately are the constraints from LFU observables, CP conserving $b \rightarrow s\mu\mu$ observables, the $B \rightarrow K^*\mu^+\mu^-$ CP asymmetries from [32], and the global fit.

In the case of $C_9^{bs\mu\mu}$, the experimental data does not lead to relevant constraints on the imaginary part of the Wilson coefficient, yet. In fact the strongest constraint on $\text{Im}(C_9^{bs\mu\mu})$ arises due to the fact that a sizeable imaginary part universally enhances the $b \rightarrow s\mu\mu$ rates. We observe that the other scenarios $\text{Im}(C_9'^{bs\mu\mu})$, $\text{Im}(C_{10}^{bs\mu\mu})$, and $\text{Im}(C_9^{bs\mu\mu}) = \text{Im}(C_{10}^{bs\mu\mu})$ are already being constrained by the experimental data on the CP asymmetries. Still, the current measurements do leave room for imaginary parts that are at least as large as the corresponding real parts. All imaginary parts are compatible with zero at the 1σ level. The best fit points of the real part of the Wilson coefficients are very close to the values that we obtain setting the imaginary parts to zero.

4. Predictions for LFU Observables and CP Asymmetries

As discussed in the previous section, several new physics Wilson coefficients (or combinations of Wilson coefficients) can significantly improve the agreement between data and theory predictions. The various best fit points show comparable pulls, and it is therefore interesting to identify predictions that allow us to distinguish the new physics scenarios.

We consider six different two parameter new physics scenarios: (i) $\text{Re } C_9^{bs\mu\mu}$ & $\text{Im } C_9^{bs\mu\mu}$, (ii) $\text{Re } C_{10}^{bs\mu\mu}$ & $\text{Im } C_{10}^{bs\mu\mu}$, (iii) $\text{Re } C_9^{bs\mu\mu} = -\text{Re } C_{10}^{bs\mu\mu}$ & $\text{Im } C_9^{bs\mu\mu} = -\text{Im } C_{10}^{bs\mu\mu}$, (iv) $C_9^{bs\mu\mu}$ & $C_{10}^{bs\mu\mu}$, (v) $C_9^{\text{univ.}}$ & $\Delta C_9^{bs\mu\mu} = -C_{10}^{bs\mu\mu}$, and (vi) $C_9^{bs\mu\mu}$ & $C_9'^{bs\mu\mu}$. In each of these cases, we sample the likelihood of the Wilson coefficients and show in Table 2 the predictions

	(i)	(ii)	(iii)	(iv)	(v)	(vi)
$R_K^{[1.1,6.0]}$	$+0.83^{+0.03}_{-0.03}$	$+0.87^{+0.03}_{-0.03}$	$+0.81^{+0.03}_{-0.03}$	$+0.81^{+0.04}_{-0.04}$	$+0.82^{+0.04}_{-0.04}$	$+0.87^{+0.03}_{-0.03}$
$R_K^{[14.18,19.0]}$	$+0.83^{+0.03}_{-0.03}$	$+0.88^{+0.03}_{-0.03}$	$+0.81^{+0.03}_{-0.03}$	$+0.82^{+0.04}_{-0.04}$	$+0.82^{+0.04}_{-0.04}$	$+0.87^{+0.03}_{-0.03}$
$R_{K^*}^{[0.045,1.1]}$	$+0.90^{+0.01}_{-0.01}$	$+0.88^{+0.01}_{-0.01}$	$+0.88^{+0.01}_{-0.01}$	$+0.89^{+0.01}_{-0.01}$	$+0.88^{+0.01}_{-0.01}$	$+0.87^{+0.01}_{-0.01}$
$R_{K^*}^{[1.1,6.0]}$	$+0.87^{+0.02}_{-0.02}$	$+0.85^{+0.03}_{-0.03}$	$+0.82^{+0.03}_{-0.03}$	$+0.85^{+0.04}_{-0.04}$	$+0.82^{+0.03}_{-0.03}$	$+0.79^{+0.03}_{-0.03}$
$R_{K^*}^{[15,19]}$	$+0.83^{+0.02}_{-0.02}$	$+0.86^{+0.03}_{-0.03}$	$+0.80^{+0.03}_{-0.03}$	$+0.81^{+0.04}_{-0.04}$	$+0.81^{+0.04}_{-0.04}$	$+0.74^{+0.03}_{-0.03}$
$R_\phi^{[1.0,6.0]}$	$+0.87^{+0.02}_{-0.02}$	$+0.86^{+0.03}_{-0.03}$	$+0.82^{+0.03}_{-0.03}$	$+0.84^{+0.04}_{-0.04}$	$+0.82^{+0.03}_{-0.03}$	$+0.78^{+0.03}_{-0.03}$
$R_\phi^{[15,19]}$	$+0.83^{+0.02}_{-0.02}$	$+0.87^{+0.03}_{-0.03}$	$+0.81^{+0.03}_{-0.03}$	$+0.81^{+0.04}_{-0.04}$	$+0.81^{+0.04}_{-0.04}$	$+0.74^{+0.03}_{-0.03}$
$D_{P'_5}^{[1.0,6.0]}$	$+0.22^{+0.04}_{-0.04}$	$-0.02^{+0.01}_{-0.01}$	$+0.08^{+0.03}_{-0.03}$	$+0.17^{+0.04}_{-0.04}$	$+0.10^{+0.03}_{-0.03}$	$+0.26^{+0.05}_{-0.05}$
$D_{P'_4}^{[1.0,6.0]}$	$+0.02^{+0.01}_{-0.01}$	$+0.03^{+0.01}_{-0.01}$	$+0.03^{+0.01}_{-0.01}$	$+0.02^{+0.01}_{-0.01}$	$+0.03^{+0.01}_{-0.01}$	$+0.02^{+0.01}_{-0.01}$
$D_{A_{FB}}^{[1.0,6.0]}$	$-0.06^{+0.02}_{-0.02}$	$+0.00^{+0.00}_{-0.00}$	$-0.03^{+0.01}_{-0.01}$	$-0.05^{+0.02}_{-0.02}$	$-0.03^{+0.01}_{-0.01}$	$-0.08^{+0.01}_{-0.01}$
$A_7^{[1.1,6]}$	$+0.00^{+0.00}_{-0.00}$	$-0.04^{+0.04}_{-0.04}$	$-0.06^{+0.03}_{-0.03}$	$+0.00^{+0.00}_{-0.00}$	$+0.00^{+0.00}_{-0.00}$	$+0.00^{+0.00}_{-0.00}$
$A_8^{[1.1,6]}$	$-0.02^{+0.01}_{-0.01}$	$+0.00^{+0.00}_{-0.00}$	$-0.03^{+0.02}_{-0.02}$	$+0.00^{+0.00}_{-0.00}$	$+0.00^{+0.00}_{-0.00}$	$+0.00^{+0.00}_{-0.00}$

Table 2: Predictions for lepton flavour universality observables and CP asymmetries in global fits of 2D new-physics scenarios as shown in figures 4, 5, and 7: (i) $\text{Re } C_9^{bs\mu\mu}$ & $\text{Im } C_9^{bs\mu\mu}$, (ii) $\text{Re } C_{10}^{bs\mu\mu}$ & $\text{Im } C_{10}^{bs\mu\mu}$, (iii) $\text{Re } C_9^{bs\mu\mu} = -\text{Re } C_{10}^{bs\mu\mu}$ & $\text{Im } C_9^{bs\mu\mu} = -\text{Im } C_{10}^{bs\mu\mu}$, (iv) $C_9^{bs\mu\mu}$ & $C_{10}^{bs\mu\mu}$, (v) $C_9^{\text{univ.}}$ & $\Delta C_9^{bs\mu\mu} = -C_{10}^{bs\mu\mu}$, (vi) $C_9^{bs\mu\mu}$ & $C_9'^{bs\mu\mu}$. The superscripts on the observables indicate the q^2 range in GeV^2 .

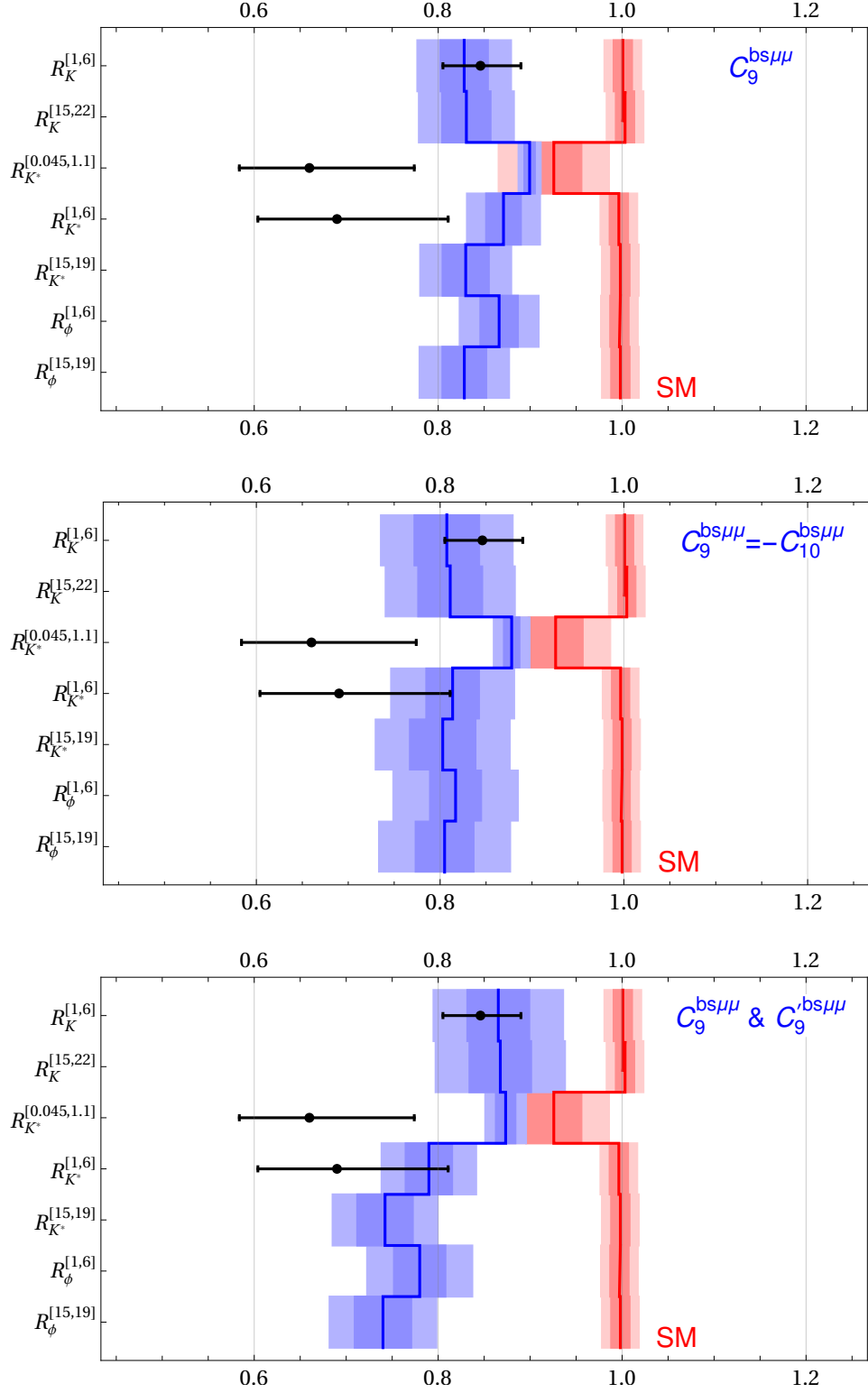


Figure 8: Predictions for the LFU ratios R_K , R_{K^*} , and R_ϕ in three new physics scenarios and the SM. For comparison the current measurements from LHCb [12,31] are shown as well.

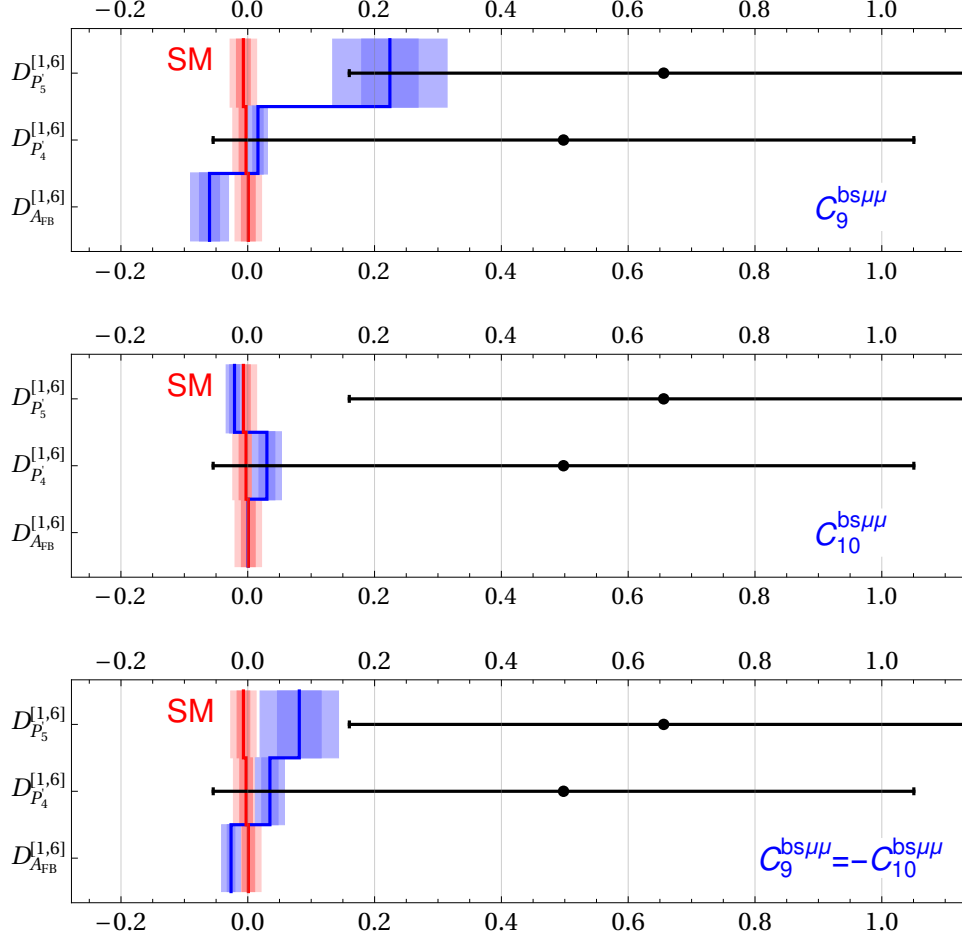


Figure 9: Predictions for the LFU differences $D_{P'_5}$, $D_{P'_4}$, and $D_{A_{FB}}$ in three new physics scenarios and the SM. For comparison the current measurements from Belle [29] are shown as well.

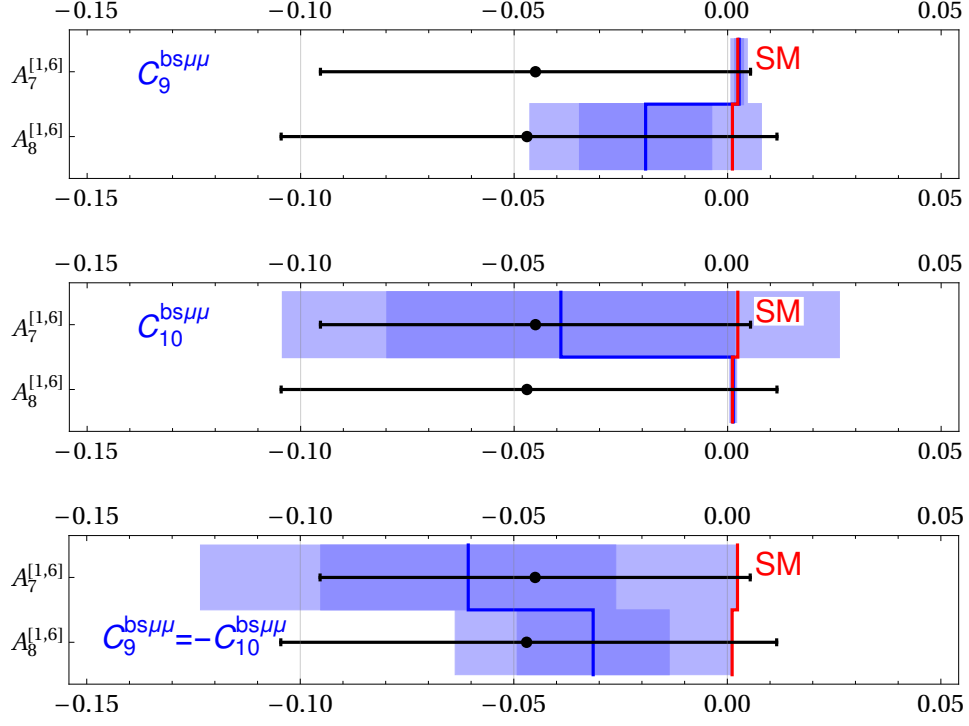


Figure 10: Predictions for the CP asymmetries A_7 and A_8 in three new physics scenarios and the SM. For comparison the current measurements from LHCb [32] are shown as well.

for several observables.

The first set of rows shows the predictions for the LFU ratios R_K , R_{K^*} , and R_ϕ both at low q^2 and at high q^2 . Overall, the predictions are fairly similar in all the considered new physics scenarios. Given the precise measurement of R_K at low q^2 that enters the global fits, all scenarios reproduce the measurement of $\simeq 0.85$ at the 1σ level. The predicted values for all other LFU ratios are similar in scenarios (i) - (v). They all are expected between 0.8 and 0.9. This is in particular true for R_{K^*} where the current experimental result is considerably lower. This conclusion does not hold in scenario (vi) that contains the right-handed Wilson coefficient $C_9'^{bs\mu\mu}$. In this case R_{K^*} can be closer to the current experimental central values.

The second set of rows shows predictions for LFU differences of $B \rightarrow K^*\mu^+\mu^-$ angular observables: $D_{P_5'}$, $D_{P_4'}$, and $D_{A_{FB}}$. Here we find significant differences in the various scenarios. In particular precise measurements of $D_{P_5'}$ will allow to narrow down new physics scenarios.

The last set of rows shows predictions for the $B \rightarrow K^*\mu^+\mu^-$ CP asymmetries A_7 and A_8 . The CP asymmetries remain close to zero (i.e. SM-like) in the scenarios (iv)-(vi) as they do not contain any new sources of CP violation. In scenarios (i)-(iii), A_7 and A_8 can be non-zero. Interestingly, an imaginary part of $C_9^{bs\mu\mu}$ leads to an effect in A_8 , while an imaginary part of $C_{10}^{bs\mu\mu}$ leads to an effect in A_7 . The predicted ranges for A_7 and A_8 can already be probed with run 2 data.

In Figures 8, 9, and 10, we show the most distinctive cases in graphical form. The plots of Figure 8 contain the predictions for the LFU ratios in scenarios (i), (iii), and (iv). The new physics predictions are compared to the SM predictions (with uncertainties from [24]) and the current experimental results [11, 31]. Similarly, the plots of Figure 9 show predictions and experimental results [29] for the LFU differences in scenarios (i), (ii), and (iii). The uncertainties of the SM predictions are illustrated with ± 0.01 . Finally, the plots of Figure 10 show the CP Asymmetries in the scenarios with imaginary parts (i), (ii), and (iii). The tiny SM uncertainties are neglected and the experimental results are taken from [32]. The plots clearly show the discrimination power of the different observables.

5. Conclusions

With the recent updates of R_K and $\text{BR}(B_s \rightarrow \mu^+\mu^-)$ by LHCb the case for new physics in rare B decays has been further strengthened. Our improved global fit shows very strong preference for the muon specific Wilson coefficients $C_9^{bs\mu\mu} \simeq -0.82$ or $C_9^{bs\mu\mu} = -C_{10}^{bs\mu\mu} \simeq$

-0.43. Even if only the theoretically clean LFU observables and $\text{BR}(B_s \rightarrow \mu^+ \mu^-)$ are considered, muon specific $C_{10}^{bs\mu\mu} \simeq 0.60$ or $C_9^{bs\mu\mu} = -C_{10}^{bs\mu\mu} \simeq -0.35$ both improve over the Standard Model by $\sqrt{\Delta\chi^2} \simeq 4.7\sigma$. We have also investigated complex Wilson coefficients and find relevant constraints on the imaginary parts of $C_{10}^{bs\mu\mu}$ and $C_9^{bs\mu\mu}$ from the experimental results on the $B \rightarrow K^* \mu^+ \mu^-$ CP asymmetries.

Finally, we give new physics predictions for large set of observables including LFU ratios, LFU differences of CP averaged $B \rightarrow K^* \mu^+ \mu^-$ observables and $B \rightarrow K^* \mu^+ \mu^-$ CP asymmetries. Future more precise measurements of these observables will allow us to distinguish between different new physics scenarios.

Note Added: Another model independent interpretation of the new results can be found in [44]. First interpretations in new physics models have been presented in [45, 46].

Acknowledgements

The research of W. A. is supported by the U.S. Department of Energy grant number DE-SC0010107.

A. Appendix: $B_q \rightarrow \mu^+ \mu^-$ Combination

We combine the ATLAS, CMS, and the recent LHCb measurement of the $B^0 \rightarrow \mu^+ \mu^-$ and $B_s \rightarrow \mu^+ \mu^-$ branching ratios [13, 16, 17], following a procedure similar as in [6].

Since the B^0 and B_s have a similar mass the measurements of the $B^0 \rightarrow \mu^+ \mu^-$ and $B_s \rightarrow \mu^+ \mu^-$ branching ratios are correlated and the experimental results are given by two-dimensional likelihoods. We combine them assuming the likelihoods of different experiments are uncorrelated. The individual likelihoods are shown as thin lines in Fig. 11 while our combination is shown as thick solid line. We also determine a Gaussian approximation (shown as thick dashed line) and compare the experimental results to the SM central values.

The two-dimensional Gaussian approximation is given by

$$\overline{\text{BR}}(B_s \rightarrow \mu^+ \mu^-)_{\text{exp}} = (2.93 \pm 0.35) \times 10^{-9}, \quad (13)$$

$$\text{BR}(B^0 \rightarrow \mu^+ \mu^-)_{\text{exp}} = (0.56 \pm 0.70) \times 10^{-10}. \quad (14)$$

with an error correlation of $\rho = -0.27$.

For the SM predictions, we use `flavio` with default settings (The most relevant input parameters are the CKM elements $V_{cb} = (42.21 \pm 0.78) \times 10^{-3}$ and $V_{ub} = (3.73 \pm 0.14) \times$

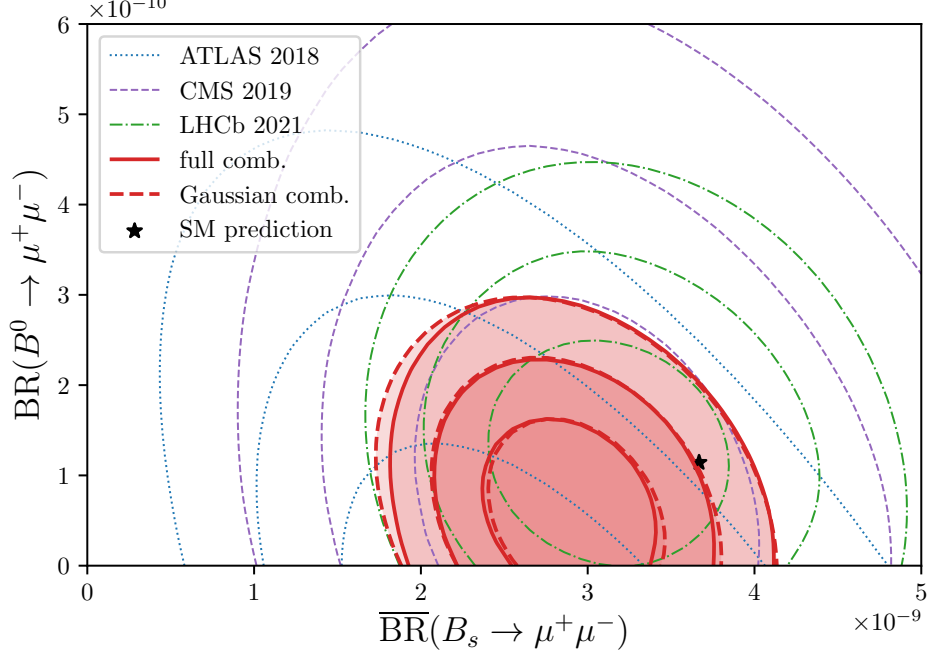


Figure 11: Likelihood contours in the plane of $\text{BR}(B^0 \rightarrow \mu^+\mu^-)$ and $\text{BR}(B_s \rightarrow \mu^+\mu^-)$ from the individual ATLAS, CMS, and LHCb measurements (thin contours), our combination (thick solid contours), and the Gaussian approximation (thick dashed contours). Also shown are the SM predictions.

10^{-3} and the decay constants $f_{B_s} = (230.3 \pm 1.3) \text{ MeV}$ and $f_B = (190.0 \pm 1.3) \text{ MeV}$ [47])

$$\overline{\text{BR}}(B_s \rightarrow \mu^+\mu^-)_{\text{SM}} = (3.67 \pm 0.15) \times 10^{-9}, \quad (15)$$

$$\text{BR}(B^0 \rightarrow \mu^+\mu^-)_{\text{SM}} = (1.14 \pm 0.12) \times 10^{-10}. \quad (16)$$

Comparing the SM predictions with the two dimensional experimental likelihood we get the following one-dimensional pulls³:

- if both branching ratios are SM-like, $2.3\sigma^4$,
- if $B_s \rightarrow \mu^+\mu^-$ is SM-like and $B^0 \rightarrow \mu^+\mu^-$ profiled over, 1.9σ ,
- if $B^0 \rightarrow \mu^+\mu^-$ is SM-like and $B_s \rightarrow \mu^+\mu^-$ profiled over, 0.8σ .

³Here, the “one-dimensional pull” is -2 times the logarithm of the likelihood ratio at the SM vs. the experimental point, after the experimental uncertainties have been convoluted with the covariance of the SM uncertainties.

⁴Converting the likelihood ratio to a pull with two degrees of freedom, we get 1.8σ ; this is why the star in Fig. 11 is very close to the 2σ contour.

Given its prominent role in constraining new physics in $b \rightarrow s\mu\mu$ transitions, it is of great interest to have confidence regions for the $B_s \rightarrow \mu^+\mu^-$ branching ratio itself, fixing $B^0 \rightarrow \mu^+\mu^-$ either to its SM central value or profiling over it. Using our two-dimensional likelihood, we find

$$\overline{\text{BR}}(B_s \rightarrow \mu^+\mu^-) = (2.93_{-0.35}^{+0.33}) \times 10^{-9} \quad \text{BR}(B^0 \rightarrow \mu^+\mu^-) \text{ profiled,} \quad (17)$$

$$\overline{\text{BR}}(B_s \rightarrow \mu^+\mu^-) = (2.86_{-0.32}^{+0.35}) \times 10^{-9} \quad \text{BR}(B^0 \rightarrow \mu^+\mu^-) \text{ SM-like.} \quad (18)$$

For $B^0 \rightarrow \mu^+\mu^-$ we get analogously

$$\text{BR}(B^0 \rightarrow \mu^+\mu^-) = (0.56_{-0.36}^{+0.70}) \times 10^{-10} \quad \overline{\text{BR}}(B_s \rightarrow \mu^+\mu^-) \text{ profiled,} \quad (19)$$

$$\text{BR}(B^0 \rightarrow \mu^+\mu^-) = (0.24_{-0.17}^{+0.72}) \times 10^{-10} \quad \overline{\text{BR}}(B_s \rightarrow \mu^+\mu^-) \text{ SM-like.} \quad (20)$$

References

- [1] L.-S. Geng, B. Grinstein, S. Jäger, J. Martin Camalich, X.-L. Ren and R.-X. Shi, *Towards the discovery of new physics with lepton-universality ratios of $b \rightarrow s\ell\ell$ decays*, *Phys. Rev. D* **96** (2017) 093006, [[1704.05446](#)].
- [2] M. Algueró, B. Capdevila, A. Crivellin, S. Descotes-Genon, P. Masjuan, J. Matias et al., *Emerging patterns of New Physics with and without Lepton Flavour Universal contributions*, *Eur. Phys. J. C* **79** (2019) 714, [[1903.09578](#)].
- [3] A. K. Alok, A. Dighe, S. Gangal and D. Kumar, *Continuing search for new physics in $b \rightarrow s\mu\mu$ decays: two operators at a time*, *JHEP* **06** (2019) 089, [[1903.09617](#)].
- [4] M. Ciuchini, A. M. Coutinho, M. Fedele, E. Franco, A. Paul, L. Silvestrini et al., *New Physics in $b \rightarrow s\ell^+\ell^-$ confronts new data on Lepton Universality*, *Eur. Phys. J. C* **79** (2019) 719, [[1903.09632](#)].
- [5] A. Datta, J. Kumar and D. London, *The B anomalies and new physics in $b \rightarrow se^+e^-$* , *Phys. Lett. B* **797** (2019) 134858, [[1903.10086](#)].
- [6] J. Aebischer, W. Altmannshofer, D. Guadagnoli, M. Reboud, P. Stangl and D. M. Straub, *B -decay discrepancies after Moriond 2019*, *Eur. Phys. J. C* **80** (2020) 252, [[1903.10434](#)].
- [7] K. Kowalska, D. Kumar and E. M. Sessolo, *Implications for new physics in $b \rightarrow s\mu\mu$ transitions after recent measurements by Belle and LHCb*, *Eur. Phys. J. C* **79** (2019) 840, [[1903.10932](#)].

- [8] T. Hurth, F. Mahmoudi and S. Neshatpour, *Implications of the new LHCb angular analysis of $B \rightarrow K^* \mu^+ \mu^-$: Hadronic effects or new physics?*, *Phys. Rev. D* **102** (2020) 055001, [[2006.04213](#)].
- [9] M. Ciuchini, M. Fedele, E. Franco, A. Paul, L. Silvestrini and M. Valli, *Lessons from the $B^{0,+} \rightarrow K^{*0,+} \mu^+ \mu^-$ angular analyses*, *Phys. Rev. D* **103** (2021) 015030, [[2011.01212](#)].
- [10] T. Hurth, F. Mahmoudi and S. Neshatpour, *Model independent analysis of the angular observables in $B^0 \rightarrow K^{*0} \mu^+ \mu^-$ and $B^+ \rightarrow K^{*+} \mu^+ \mu^-$* , [2012.12207](#).
- [11] LHCb collaboration, R. Aaij et al., *Test of lepton universality in beauty-quark decays*, [2103.11769](#).
- [12] LHCb collaboration, R. Aaij et al., *Search for lepton-universality violation in $B^+ \rightarrow K^+ \ell^+ \ell^-$ decays*, *Phys. Rev. Lett.* **122** (2019) 191801, [[1903.09252](#)].
- [13] LHCb collaboration, M. Santimaria, *LHC Seminar “New results on theoretically clean observables in rare B-meson decays from LHCb”, 23 March, 2021*, https://indico.cern.ch/event/976688/attachments/2213706/3747159/santimaria_LHC_seminar_2021.pdf.
- [14] ATLAS, CMS, AND LHCb collaboration, *Combination of the ATLAS, CMS and LHCb results on the $B_{(s)}^0 \rightarrow \mu^+ \mu^-$ decays*, .
- [15] LHCb collaboration, R. Aaij et al., *Measurement of the $B_s^0 \rightarrow \mu^+ \mu^-$ branching fraction and effective lifetime and search for $B^0 \rightarrow \mu^+ \mu^-$ decays*, *Phys. Rev. Lett.* **118** (2017) 191801, [[1703.05747](#)].
- [16] ATLAS collaboration, M. Aaboud et al., *Study of the rare decays of B_s^0 and B^0 mesons into muon pairs using data collected during 2015 and 2016 with the ATLAS detector*, *JHEP* **04** (2019) 098, [[1812.03017](#)].
- [17] CMS collaboration, A. M. Sirunyan et al., *Measurement of properties of $B_s^0 \rightarrow \mu^+ \mu^-$ decays and search for $B^0 \rightarrow \mu^+ \mu^-$ with the CMS experiment*, *JHEP* **04** (2020) 188, [[1910.12127](#)].
- [18] R. Alonso, B. Grinstein and J. Martin Camalich, *$SU(2) \times U(1)$ gauge invariance and the shape of new physics in rare B decays*, *Phys. Rev. Lett.* **113** (2014) 241802, [[1407.7044](#)].

- [19] S. Jäger, M. Kirk, A. Lenz and K. Leslie, *Charming new physics in rare B-decays and mixing?*, *Phys. Rev. D* **97** (2018) 015021, [[1701.09183](#)].
- [20] A. Crivellin, C. Greub, D. Müller and F. Saturnino, *Importance of Loop Effects in Explaining the Accumulated Evidence for New Physics in B Decays with a Vector Leptoquark*, *Phys. Rev. Lett.* **122** (2019) 011805, [[1807.02068](#)].
- [21] W. Altmannshofer and D. M. Straub, *New physics in $b \rightarrow s$ transitions after LHC run 1*, *Eur. Phys. J. C* **75** (2015) 382, [[1411.3161](#)].
- [22] W. Altmannshofer, C. Niehoff, P. Stangl and D. M. Straub, *Status of the $B \rightarrow K^* \mu^+ \mu^-$ anomaly after Moriond 2017*, *Eur. Phys. J. C* **77** (2017) 377, [[1703.09189](#)].
- [23] W. Altmannshofer, P. Stangl and D. M. Straub, *Interpreting Hints for Lepton Flavor Universality Violation*, *Phys. Rev. D* **96** (2017) 055008, [[1704.05435](#)].
- [24] M. Bordone, G. Isidori and A. Pattori, *On the Standard Model predictions for R_K and R_{K^*}* , *Eur. Phys. J. C* **76** (2016) 440, [[1605.07633](#)].
- [25] G. Isidori, S. Nabeebaccus and R. Zwicky, *QED corrections in $\overline{B} \rightarrow \overline{K} \ell^+ \ell^-$ at the double-differential level*, *JHEP* **12** (2020) 104, [[2009.00929](#)].
- [26] J. Albrecht, F. Bernlochner, M. Kenzie, S. Reichert, D. Straub and A. Tully, *Future prospects for exploring present day anomalies in flavour physics measurements with Belle II and LHCb*, [1709.10308](#).
- [27] W. Altmannshofer and I. Yavin, *Predictions for lepton flavor universality violation in rare B decays in models with gauged $L_\mu - L_\tau$* , *Phys. Rev. D* **92** (2015) 075022, [[1508.07009](#)].
- [28] B. Capdevila, S. Descotes-Genon, J. Matias and J. Virto, *Assessing lepton-flavour non-universality from $B \rightarrow K^* \ell \ell$ angular analyses*, *JHEP* **10** (2016) 075, [[1605.03156](#)].
- [29] BELLE collaboration, S. Wehle et al., *Lepton-Flavor-Dependent Angular Analysis of $B \rightarrow K^* \ell^+ \ell^-$* , *Phys. Rev. Lett.* **118** (2017) 111801, [[1612.05014](#)].
- [30] G. Hiller and M. Schmaltz, *Diagnosing lepton-nonuniversality in $b \rightarrow s \ell \ell$* , *JHEP* **02** (2015) 055, [[1411.4773](#)].

- [31] LHCb collaboration, R. Aaij et al., *Test of lepton universality with $B^0 \rightarrow K^{*0} \ell^+ \ell^-$ decays*, *JHEP* **08** (2017) 055, [[1705.05802](#)].
- [32] LHCb collaboration, R. Aaij et al., *Angular analysis of the $B^0 \rightarrow K^{*0} \mu^+ \mu^-$ decay using 3 fb^{-1} of integrated luminosity*, *JHEP* **02** (2016) 104, [[1512.04442](#)].
- [33] C. Bobeth, G. Hiller and G. Piranishvili, *CP Asymmetries in $\bar{B} \rightarrow \bar{K}^*(\rightarrow \bar{K} \pi) \bar{\ell} \ell$ and Untagged $\bar{B}_s, B_s \rightarrow \phi(\rightarrow K^+ K^-) \bar{\ell} \ell$ Decays at NLO*, *JHEP* **07** (2008) 106, [[0805.2525](#)].
- [34] W. Altmannshofer, P. Ball, A. Bharucha, A. J. Buras, D. M. Straub and M. Wick, *Symmetries and Asymmetries of $B \rightarrow K^* \mu^+ \mu^-$ Decays in the Standard Model and Beyond*, *JHEP* **01** (2009) 019, [[0811.1214](#)].
- [35] LHCb collaboration, R. Aaij et al., *Measurement of CP-Averaged Observables in the $B^0 \rightarrow K^{*0} \mu^+ \mu^-$ Decay*, *Phys. Rev. Lett.* **125** (2020) 011802, [[2003.04831](#)].
- [36] LHCb collaboration, R. Aaij et al., *Angular analysis of the $B^+ \rightarrow K^{*+} \mu^+ \mu^-$ decay*, [2012.13241](#).
- [37] K. De Bruyn, R. Fleischer, R. Knegjens, P. Koppenburg, M. Merk, A. Pellegrino et al., *Probing New Physics via the $B_s^0 \rightarrow \mu^+ \mu^-$ Effective Lifetime*, *Phys. Rev. Lett.* **109** (2012) 041801, [[1204.1737](#)].
- [38] W. Altmannshofer, C. Niehoff and D. M. Straub, *$B_s \rightarrow \mu^+ \mu^-$ as current and future probe of new physics*, *JHEP* **05** (2017) 076, [[1702.05498](#)].
- [39] PARTICLE DATA GROUP collaboration, P. A. Zyla et al., *Review of Particle Physics*, *PTEP* **2020** (2020) 083C01.
- [40] D. M. Straub, *flavio: a Python package for flavour and precision phenomenology in the Standard Model and beyond*, [1810.08132](#).
- [41] J. Aebischer, J. Kumar, P. Stangl and D. M. Straub, *A Global Likelihood for Precision Constraints and Flavour Anomalies*, *Eur. Phys. J. C* **79** (2019) 509, [[1810.07698](#)].
- [42] P. Stangl, *smelli – the SMEFT Likelihood*, in *Tools for High Energy Physics and Cosmology*, 12, 2020, [2012.12211](#).
- [43] N. Gubernari, D. Van Dyk and J. Virto, *Non-local matrix elements in $B_{(s)} \rightarrow \{K^{(*)}, \phi\} \ell^+ \ell^-$* , *JHEP* **02** (2021) 088, [[2011.09813](#)].

- [44] L.-S. Geng, B. Grinstein, S. Jäger, S.-Y. Li, J. M. Camalich and R.-X. Shi, *Implications of new evidence for lepton-universality violation in $b \rightarrow s\ell^+\ell^-$ decays*, [2103.12738](#).
- [45] A. Angelescu, D. Bečirević, D. A. Faroughy, F. Jaffredo and O. Sumensari, *On the single leptoquark solutions to the B -physics anomalies*, [2103.12504](#).
- [46] G. Hiller, D. Loose and I. Nišandžić, *Flavorful leptoquarks at the LHC and beyond: Spin 1*, [2103.12724](#).
- [47] FLAVOUR LATTICE AVERAGING GROUP collaboration, S. Aoki et al., *FLAG Review 2019: Flavour Lattice Averaging Group (FLAG)*, *Eur. Phys. J. C* **80** (2020) 113, [[1902.08191](#)].